Accepted Manuscript

The mechanism of rate-dependent off-axis compression of a low fibre volume fraction thermoplastic matrix composite

Michael I. Okereke, C. Paul Buckley, Ambrose I. Akpoyomare

PII: S0263-8223(16)32418-7
DOI: http://dx.doi.org/10.1016/j.compstruct.2017.02.070
Reference: COST 8292

To appear in: *Composite Structures*

Received Date: 3 November 2016
Revised Date: 8 January 2017
Accepted Date: 10 February 2017

Please cite this article as: Okereke, M.I., Paul Buckley, C., Akpoyomare, A.I., The mechanism of rate-dependent off-axis compression of a low fibre volume fraction thermoplastic matrix composite, *Composite Structures* (2017), doi: http://dx.doi.org/10.1016/j.compstruct.2017.02.070

1.

The mechanism of rate-dependent off-axis compression of a low fibre volume fraction thermoplastic matrix composite.

Michael I. Okereke[a,*], C. Paul Buckley[b], Ambrose I. Akpoyomare[a]

[a]*Department of Engineering Science, University of Greenwich, Kent, United Kingdom*
[b]*Department of Engineering Science, University of Oxford, Oxford, OX1 3PJ*

Abstract

This paper reports on the mechanism of rate-dependent off-axis compression of a unique unidirectional composite with unusually high matrix volume fraction of 65%. The test material is an E-glass fibre reinforced polypropylene composite and was subjected to quasi-static, medium and high strain rates (with strain rates from 10^{-3} s^{-1} to 10^{3} s^{-1}). This paper has shown experimental evidence of significant rate-dependence of yielding, strain softening and fracture strain of the test composite. Also, the study reports on the effect of strain rates on evolution of different failure modes of the composite. The observed rate-dependence was shown to result from the influence of the pure matrix on the constitutive behaviour of the composite. The work has used a *two-process Ree-Eyring* yield model of the matrix to demonstrate the origin of the observed rate-dependent yielding of the composite. The data derived in this study will be significant for further micro-mechanical modelling of finite deforming composites used in especially damage tolerant applications. Composite design engineers and stress analysis experts should benefit also from the findings in this work.

Keywords: Thermoplastic matrix composites, Impact behaviour, Rate-dependence, Finite deformation, High strain rates.

1. Introduction

Polymer matrix composites have found wide ranging and increasing application in airplanes, spacecraft, light weight structures, medical prosthesis, sandwich structures and sports equipment manufacture industries. In many of these applications, thermoset composites are commonplace but in the last two decades, thermoplastic matrix composites have become prevalent particularly in applications where high damage tolerance is a design

Corresponding Address: Department of Engineering Science, University of Greenwich, Medway Campus, Kent, ME4 4TB, United Kingdom Phone: +44 (0) 1634 88 3580 Fax: +44 (0) 1634 88 3153.
Email address: m.i.okereke@gre.ac.uk (Michael I. Okereke)

requirement. Most of the advantages of thermoplastic matrix composites over thermoset composites stem from their ease of processing, excellent damage tolerance characteristics [1], high strength-to-weight ratios and good impact energy absorption [2]. Existing research on such composites have been dedicated to improving their processing capabilities to encourage their uptake in aero, auto and sports/leisure industries [3–8].

The initial uses of thermoplastic matrix composites was restricted to semi-structural applications such as door panels. However, in recent times, there has been significant progress in the manufacturing processes of the thermoplastic matrix composites through the injection moulding of complex geometries. This has increased their use in structural applications such as vehicle bumpers, and crash structures. In fact, glass fibre reinforced polypropylene (GFRP) is a key composite used essentially in design of car bumpers, boat hulls, wind turbine blades and other automotive applications [9]. This means that the composites are therefore subjected to high loading rates where understanding the impact resistance is important. The rate-dependent mechanical properties of the test composite will always be required in predictive modelling of structural applications involving crashworthiness and post-impact behaviour prediction [10]. A study by Carrillo and co-workers [11] considered the ballistic behaviour of a thermoplastic composite with a polypropylene matrix and the authors found that the properties of the matrix improved the ballistic performance of the composites.

There is a large body of data on off-axis impact response of composite structures especially the carbon-epoxy material systems used in aerospace applications [12–16]. However, the number of such studies on off-axis compression of thermoplastic matrix composites is limited. Brown and co-workers [17] studied both static and high rate behaviour of commingled E-glass/polypropylene woven fabric composites using tensile, compression and shear tests. The composite has a 60% weight fraction of fibre hence the fibre properties dominated the response. Similarly, Hufenbach *et al.* [18] have accumulated extensive experimental data for polypropylene/glass-fibre 3D-textile reinforced composite, using tensile, charpy impact, open-hole tensile and dynamic mechanical analysis tests. This textile composite had a matrix volume fraction of about 50% hence the fibre properties dominated the constitutive behaviour. In fact, in the transverse directions, the compressive behaviour was dominated by linear viscoelasticity.

However, there is no data in literature for the high matrix volume fraction compression moulded continuous fibre, unidirectional, E-glass/polypropylene composite studied here. Even though traditional uses of composites in structural applications require higher fibre volume fraction where accurate representation of the matrix phase is not required, there is an increasing example of low fibre volume fraction composites about. Such composites are particularly required for damage tolerant applications where the finite deformation of the composite is essential for significant energy absorption. For these composites, it is necessary that a detailed modelling of the high matrix volume fraction phase is carried out. The constitutive behaviour of the composite will be expected to show the classic nonlinear viscoelasticity of the dominant PP matrix constituent thereby leading to a finite deforming off-axis compressive behaviour of the composite. This will require different predictive modelling approaches compared with traditional high fibre volume fraction composites. Test data have been generated from tests in two matrix-dominated off-axis directions namely 45^o- and 90^o-directions. Compression tests along the longitudinal (fibre) direction is dominated by the often comparably less rate-dependent fibre response and so have been excluded in this work. The paper also discusses the rate-dependence of yield, strain softening, fracture strain and the failure mechanisms of the composite.

2. Test Material

2.1. The thermoplastic matrix composite

The test material for this study is a highly oriented thermoplastic matrix composite called Plytron™ [1] - the registered trademark for 100% consolidated continuous unidirectional E-glass fibre reinforced polypropylene composite. Plytron™ is commercially available as prepreg tapes of 300 mm wide, 0.25 - 0.28 mm thick and roll length of 400 m [19, 20]. According to the manufacturer's documentation [19, 20], the fibre reinforcement is isotropic E-glass fibre and the matrix is polypropylene: a semicrystalline polymer mixed with a proprietary master-batch compound. The exact composition of the master-batch is unknown, but it makes up about 5% volume fraction of the entire bulk and contains carbon-black fillers. The master-batch was added to improve the consolidation of the composite and to also enhance the aesthetics of the composite. Table 1 shows the mechanical properties of the ingredients used in Plytron™ . Our choice of Plytron™ in this study stems from its unusually high matrix volume fraction of 65% (comprising 60% polypropylene and 5% master-batch compound).

Table 1: Typical room temperature properties of E-glass fibre reinforcement and isotropic semicrystalline polypropylene matrix used in Plytron™ [19].

Property	Fibre	Matrix	Units
Density, ρ	2600	900	kg/m^3
Young's Modulus, E	73	1.308	GPa
Tensile Strength, X	2250	40	MPa
Shear Modulus, G	31	0.46	GPa

2.2. Manufacture of Test material

Unidirectional composite laminates were prepared from Plytron prepreg tapes through compression moulding. Cogswell *et al.* [21] described the technology for production of such prepregs by melt-impregnation of fibre tows. High consolidation, essential for obtaining good mouldings, involves two sub-processes: removal of air from the interface of the prepreg tapes to alleviate voiding, and adhesion of the prepregs, as heat and pressure are applied. A specially made mould was used for the compression moulding. The optimum processing conditions for preparing well consolidated laminates were: (a) temperature (of heated

[1]The test material was originally manufactured and marketed by Gurit Suprem but now trades as Gurit. The production of Plytron™ has now been discontinued by Gurit.

platens): $22^o - 250°$ C, (b) pressure applied on top and bottom of the mould: 1.5 − 2.0 MPa, (c) number of plies per 10 mm thick laminate: 43 plies[2], and (d) processing cycle time: 25 mins (comprising 10 mins heating up, 5 mins dwell time and 10 mins cooling period). Typical heating and cooling rates were 15° C/min and 20° C/min respectively. The mould was cooled from the set temperature to room temperature by water cooling of the heated platens. The stacking sequence of laminates was: $[0_{43}]$, while ensuring that each of the prepregs was aligned with the main fibre axis of all prepregs. After the moulding cycle, well consolidated circular discs of diameter, d = 100 mm and thickness, t = 10 mm were obtained.

3. General Experimental Setup

3.1. Design of Test Specimens

Cubic test specimens, illustrated in *Figure 1*, were machined from each circular laminate disc, with the normal to the loaded face of the cube at either 90^o or 45^o to the fibre directions. The 90^o-specimens were of dimensions: $8 \times 8 \times 8$ mm^3 while the 45^o-specimens were of dimensions $10 \times 10 \times 10$ mm^3. The surfaces of the test specimens were carefully polished and lapped until flat test surfaces were obtained. The matrix (i.e. polypropylene) is very brittle in tension, at room temperature, which can cause edges of the laminates to break off easily during polishing. Therefore, care was taken to ensure that the specimens remained perfectly cubic during and after the polishing process.

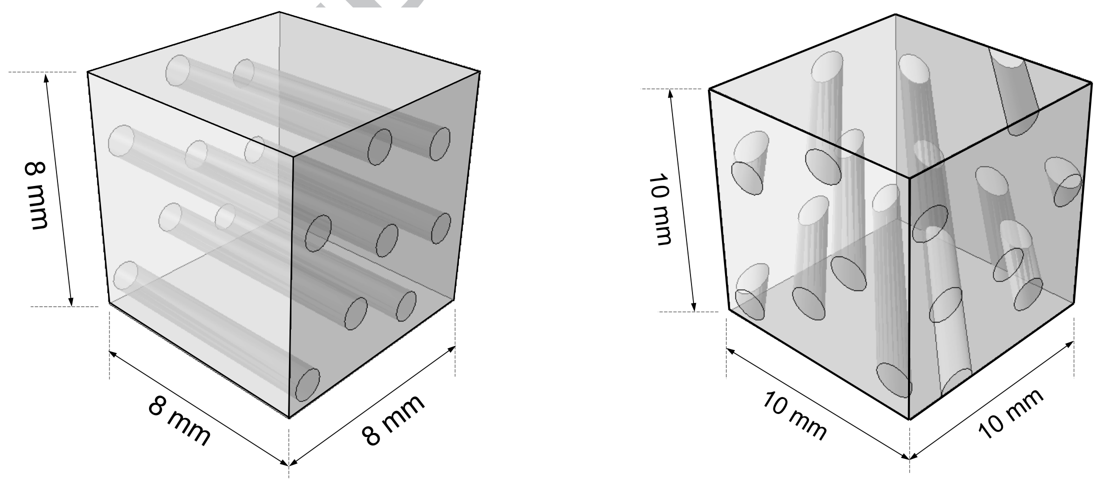

(a) (b)

Figure 1: Specimen designs used for two off-axis testing directions namely: (a) 90^o- and (b) 45^o.

3.2. Quasi-static test setup

All quasi-static compression tests[3] were performed in a screw-driven Hounsfield testing machine fitted with CMOS cameras for *in situ* imaging The CMOS camera is a 4-megapixel

[2] Each ply is a circular disc of prepreg, of dimensions: diameter, d = 100 mm, average thickness, t = 0.26 mm.

[3] Quasi-static strain rates are defined as: 10^{-4} s^{-1} $\leq \epsilon \leq 10^{-1}$ s^{-1}

camera set capable of acquiring images at a speed of one frame per second. Visualization data obtained from the camera were used to observe the compressive behaviour of the thermoplastic matrix composites and these are discussed later in *Section 6*. The Hounsfield testing machine was fitted with a laser extensometer with a precision of 10 μm, which gave displacement measurements. The distance between thin white stripes painted on the ends of the anvils were tracked by the laser extensometer and the true strain measurements, reported in *Section 4*, were based on the tracked distances. Finally, total resisting force on the specimen was derived based on a 100 kN load cell.

3.3. Medium rate test setup

Tests at the medium rates[4] were performed using a hydraulic/piston-driven test rig (as shown in *Figure 2*). The test rig can nominally achieve strain rates ranging from $1 - 500$ s^{-1}, although in the present work 50 s^{-1} was the maximum rate achieved. Force signals

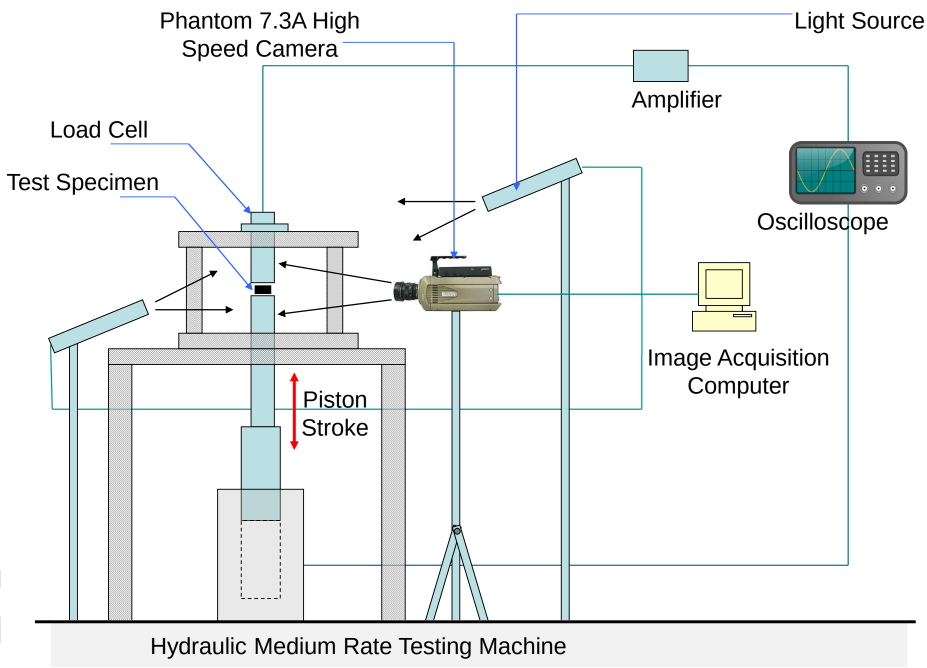

Figure 2: Schematic representation of the hydraulic/piston-driven medium rates test rig and allied data/image acquisition accessories

were recorded using a load cell, and at the strain rates used in this work, the signal suffered no significant distortion from load cell ringing or other perturbations. Stress-time plots were obtained from the force signals[5] and the initial surface areas of the test specimens. A Phantom 7.3A high speed camera was attached to the test rig to provide in situ images of the deforming composite. Displacement of thin white stripes painted on the test anvils, close to the specimen, were tracked using images acquired from the camera. These pixel-based

[4]In this study, medium rates are defined as strain in the range of: 10^{o} s^{-1} $\leq \epsilon$ 10^{2} s^{-1}

[5]Force signals were recorded in voltage but were converted to Newton units using appropriate calibration data.

measurements were calibrated in the region of the gauge length, h_0 and converted to true strain using an in-house MATLAB algorithm.

3.4. High rate test setup

A compression split Hopkinson pressure bar (SHPB) was used to study the high rate compressive response of the thermoplastic matrix composites. The arrangement of all accessories around the SHPB used in this work is shown in *Figure 3*. The cylindrical impactor is 250 mm long and 16 mm in diameter. It impacts a maraging steel input bar, 500 mm long and 15 mm in diameter, at a speed ranging from 10 to 20 ms^{-1}. Two strain gauges (marked as G1 & G2 in *Figure 3*) were used to record the input stress waves. These gauges were located at 308 mm and 40 mm from the specimen respectively. Since two strain gauge signals were obtained from the input bar (in comparison with the traditional single strain gauge input signal in most SHPBs), a wave separation analysis was performed to calculate the input and reflected waves from the gauge signals [22–25]. The output bar is a 459 mm long, 15 mm diameter maraging steel bar, instrumented with a single gauge located 40 mm from the test specimen end of the bar. Gauge G3 was used to record the stress waves on the output bar.

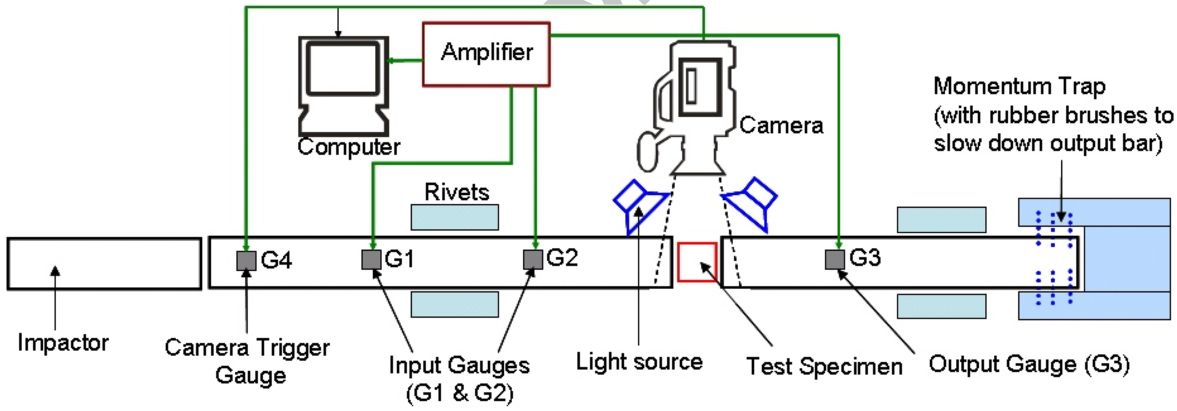

Figure 3: Schematic diagram of a compression SHPB showing a high-speed camera used for acquiring *in situ* images of deforming composite.

Typical bar signals derived from gauges G_1 to G_3 and the associated rise times for each signal are given in *Figure 4(a)*. Using appropriate calibration parameters, the bar signals can be converted to stress measures and ends-of-bar displacements used to determine strain measurements. *Figure 4(b)* demonstrates that in the region around yield, the test specimen was subjected to a near constant strain rate, which is essential if the stress-strain data obtained from the split Hopkinson pressure bar setup is to be used as model validation data for constitutive models of the test composite.

In high rate studies involving the split Hopkinson pressure bar, it is important to consider whether the tested specimen has reached mechanical equilibrium within the short timescales. This study also explored this issue by comparing the sample stress derived from the transmitted wave with that of the algebraic sum of the incident wave and reflected wave. The later stress is often noisier because of the signal subtraction involved during the wave

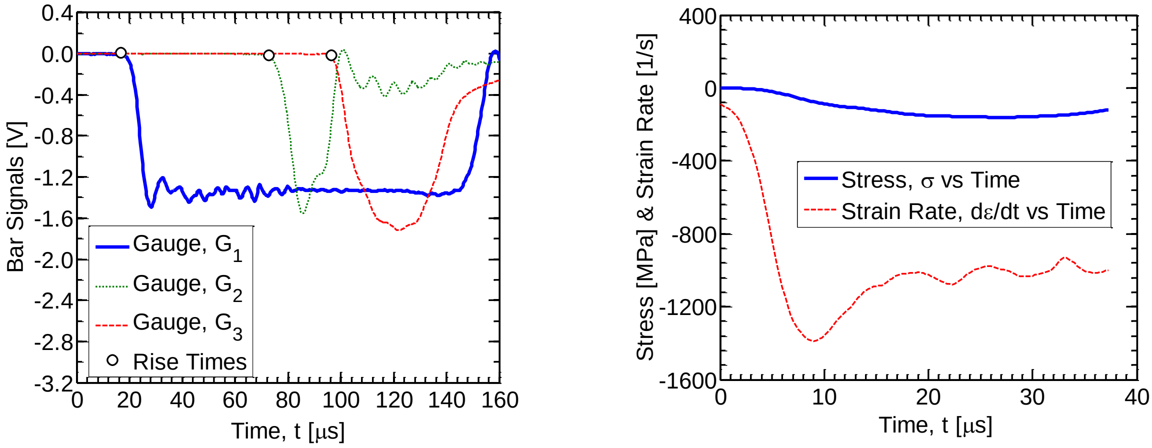

(a) (b)

Figure 4: (a) Bar signals derived from gauges G_1, G_2 and G_3 with their rise times; and (b) a comparison of strain rate and stress measures derived from a split Hopkinson pressure bar tests.

separation analysis [22, 26]. The two stresses were found to agree within the allowable noise of the later data, demonstrating achievement of mechanical equilibrium in each case. *Figures 5(a)* and *5(b)* show typical examples of mechanical equilibrium for the 45^o and 90^o test directions at strain rates of 2000 s^{-1} and 2166 s^{-1} respectively.

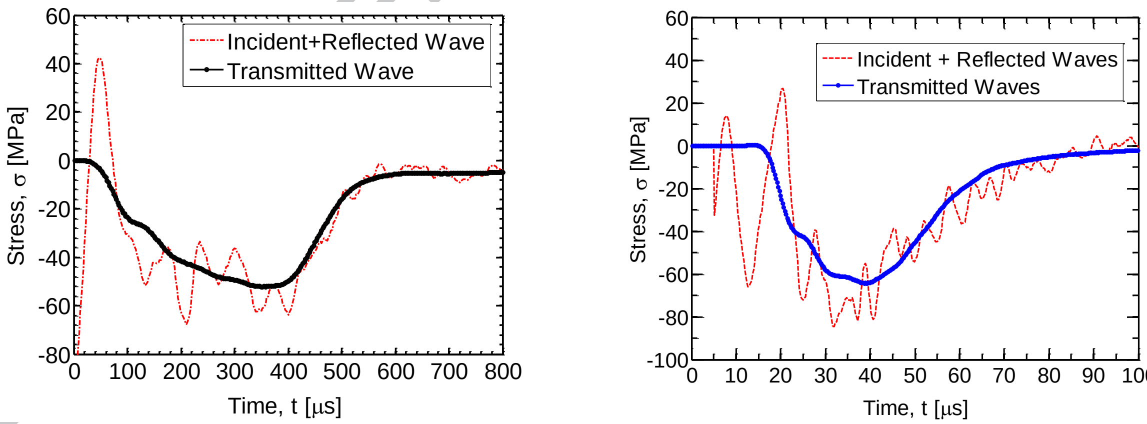

(a) (b)

Figure 5: Establishing mechanical equilibrium in a split Hopkinson pressure bar setup for compression tests in two off-axis directions: (a) 45^o (strain rate, $\dot{\epsilon} = 2000s^{-1}$) and (b) 90^o direction to the main fibre axis (strain rate, $\dot{\epsilon} = 2166s^{-1}$).

As shown in *Figure 3*, a high speed camera was also attached to the SHPB to image the deforming test composite at the impact rates. The high speed camera used is a Cordion 550 rotating mirror CCD camera. The camera captures 62 frames, each of 1 mega-pixel resolution, up to a frame rate of 4 million frames per second. To synchronize the camera with the start of deformation, the camera was triggered externally using square-wave input signals taken from gauge G4, placed 400 mm away from the specimen.

4. Test results

The results of off-axis compression tests across quasi-static, medium and high strain rates are shown in *Figures 6* and *7* for 45^o and 90^o off-axis directions respectively. Nominal stresses were obtained by assuming incompressibility. A similar result for the compressive response of the exact filled polypropylene grade used as matrix in Plytron™ has been published by Okereke *et al.*[27] and stress-strain plots for that grade of polypropylene are shown in *Figure 8*.

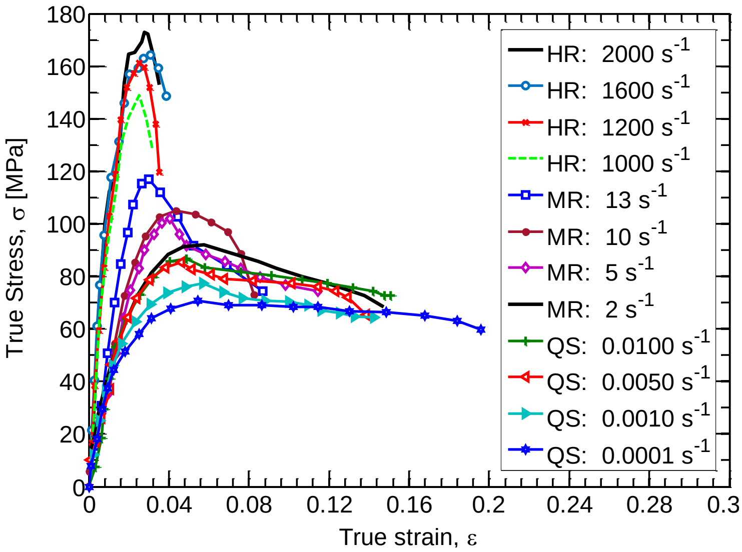

Figure 6: Rate-dependent off-axis compression of Plytron™ for 45^o direction.*Note: HR - high rate, MR-medium rate and QS - quasi-static.*

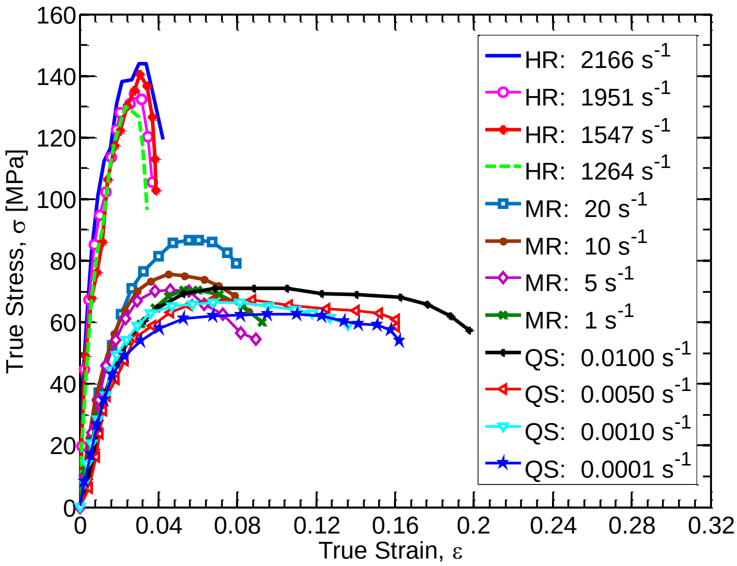

Figure 7: Rate-dependent off-axis compression of Plytron™ for 90^o direction. *Note: HR - high rate, MR-medium rate and QS - quasi-static.*

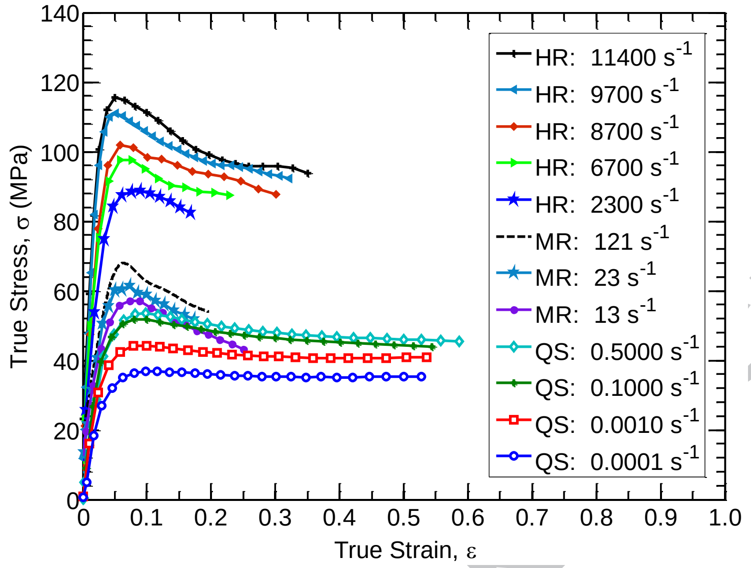

Figure 8: Rate-dependent off-axis compression of polypropylene matrix used in Plytron™ after Okereke *et al.*[27]. *Note: HR - high rate, MR-medium rate and QS - quasi-static.*

It can be concluded that the compression test results for the composite are comparable to the results for the bulk matrix (polypropylene). In all cases there is a rate-dependent non-linear response, characteristic of viscoelasticity, and a definite peak in true stress, here taken as the apparent 'yield' point. With respect to tests in the 45^o-direction, the apparent yield stress increased from 70 MPa (at quasi-static strain rate, $\dot{\epsilon} = 10^{-4}$ s^{-1}) to 175 MPa (at high strain rate, $\dot{\epsilon} = 2000$ s^{-1}) with increasing strain rate. Similarly, the apparent yield stress for the 90^o-direction specimens increased from 60 MPa to 145 MPa across seven decades of strain rate. The similarity of the stress-strain graphs between the matrix-only compression (*Figure 8*) and Plytron™ (*Figures 6* and *7*) leads the authors to conclude that the matrix rate-dependent response determines the observed composite rate-dependence. This is consistent with observations for similar thermoplastic matrix composites [17, 28, 29]. All these demonstrate that the off-axis compressive response of the chosen thermoplastic matrix composites varies with changing strain rates because of the rate-dependence of the thermoplastic polymer matrix.

5. Discussion

5.1. The mechanics of rate-dependent yielding of the composite

The test results of *Section 4* show a rate-dependent yielding of the test composite with, for example the test results of 45^o-direction compression, showing a change of yield stress from 70 MPa at $\dot{\epsilon} = 0.0001$ s^{-1} to 170 MPa at $\dot{\epsilon} = 2000$ s^{-1}. In this section, we provide a discussion of the origin and mechanics of this rate-dependence.

Consider an idealized unidirectional (UD) composite where the fibre points in the $3-$axis whilst the two transverse directions are $1-$ and $2-$axes respectively as shown in *Figure 9(a)*. It is assumed that (1) fibres are linear elastic and (b) matrix is nonlinear viscoelastic with the yield stress defined by *Ree-Eyring* rate kinetics [30–34].

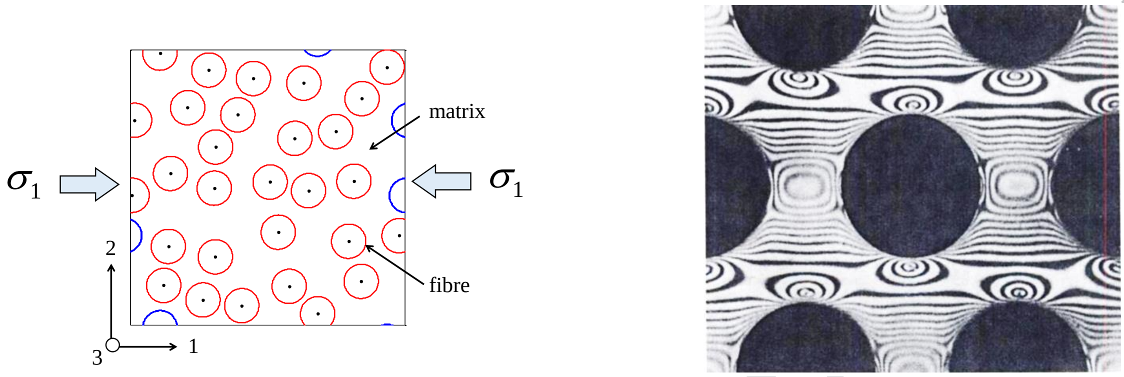

(a) (b)

Figure 9:
(a) Schematic of a typical representative volume element (RVE) of a UD composite subjected to a $1-$axis transverse loading, σ_1. *Note that the fibres are represented by circles and the square box is the matrix.*

(b) Illustration of nonlinear matrix stress distribution with contours of principal stress difference in $1-2$ plane using a photoelastic image of a macromodel composite under tensile loading in vertical direction. Black regions show the fibres. *Image reproduced with kind permission of Hull and Clyne* [35].

Consider the compression at 90^o to fibres at constant strain rate along the $1-$axis, $\dot{\epsilon}_1$ as shown in *Figure 9(a)*. Since the fibres are continuous and much stiffer than the matrix, the strain rate or strain in the fibre will be quite small in comparison with strain rate (or strains) in the two transverse directions. As a result, this compression test is assumed to be a plane strain problem hence: $\dot{\epsilon} = \epsilon = 0$. At low values of stress, $\sigma_1 \rightarrow 0$, the matrix is elastic but stress across the microstructure is non-uniform as shown in *Figure 9(b)*.

With increasing compressive loading, the matrix stress distribution continues to increase as well until the matrix yields at a stress, σ_1^0, in the vicinity of a stress concentration, resulting from the plastic zone. This is shown schematically in *Figure 10(a)*. With further increases in transverse compressive stress σ_1, the plastic zones continue to grow until there is a *percolation of plastic zones* through out the matrix, providing a mechanism for plastic collapse of the structure i.e. the composite 'yields' at a reference stress. This is assumed as a deformation at constant stress of the composite. The critical stress, σ_1^* becomes the apparent yield stress of the composite in this test. A graphical sketch of a typical stress-strain plot illustrating this is shown in *Figure 11*.

In order to describe objectively the apparent yielding of the matrix (in the percolated state), we invoke the widely accepted *Ree-Eyring* rate kinetics used for modelling rate-dependence in polymeric systems. The authors here adopt a variant of the Ree-Eyring model (called the *two-process model*) proposed previously by Okereke *et. al* [36] for modelling three grades of polypropylene, including the filled polypropylene matrix of Plytron. The model proposes that the flow/yield stress for polymers or polymer-based materials is a co-operative

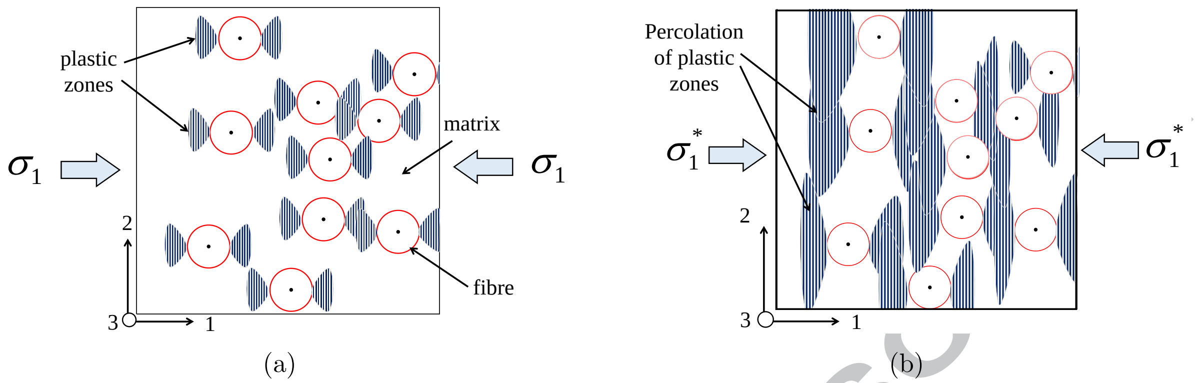

Figure 10: A schematic representation of the development of plastic zones for a macromodel of the composite subjected to transverse (1−axis) compression, showing: (a) onset and (b) percolation of the plastic zones.

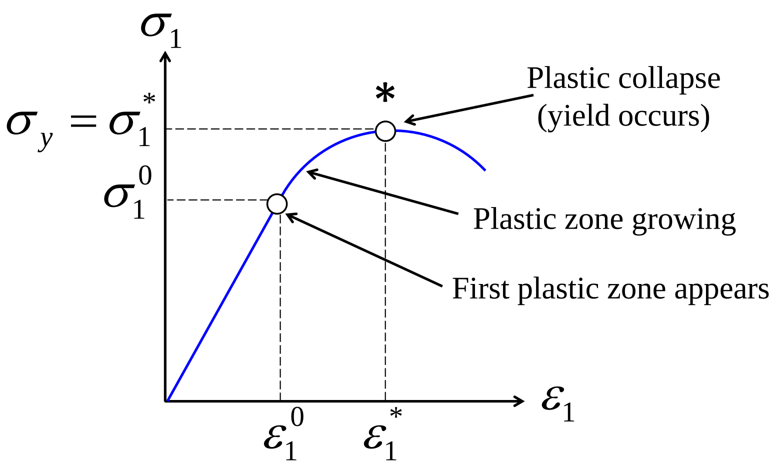

Figure 11: Stress-strain plot showing evolution of plastic zones and associated parameters.

interaction of two viscoelastic relaxation processes. At room temperature, the first process is dominant at quasi-static rates with near insignificant contribution of the second process. After a critical strain rate, $\dot{\epsilon}^{crit}$ is exceeded, the second process begins to grow rapidly. According to Okereke *et. al* [36], the equations describing the two co-operating viscoelastic relaxation processes for the matrix (polypropylene) are given as follows:

$$\sigma_{y,\text{process I}} = \frac{6RT}{\sqrt{2}V_{s,j} - 2V_{p,j}} \left\{ \ln A_j + \ln |\dot{\epsilon}| \right\} \tag{1}$$

$$\sigma_{y,\text{process II}} = \frac{6RT}{\sqrt{2}V_{s,j} - 2V_{p,j}} \ln \left\{ \frac{\gamma_j A_j \dot{\epsilon}}{2} + \sqrt{\left(\frac{\gamma_j A_j \dot{\epsilon}}{2}\right)^2 + 1} \right\} \tag{2}$$

where $R =$ gas constant, $T =$ temperature, $j = I$ or II, where I and II refer to the $\alpha-$ and $\beta-$ viscoelastic relaxations in polypropylene, A_j and γ_j are material constants, $V_{s,j}$ and $V_{p,j}$ are shear and pressure activation volumes for the $j-$ viscoelastic relaxation. Hence the predicted total yield stress:

$$\sigma_y = \sigma_{y,\text{process I}} + \sigma_{y,\text{process II}}. \tag{3}$$

Since the yielding of the composite is a consequence of the percolation of the plastic zones formed in the matrix region and the fibre constituents exist as stiff/hard inclusions (see *Figure 9(a)*), then we extrapolate that the rate-dependent yielding of the composite will follow same mechanism as the matrix. We draw confidence, to make this extrapolation, in the similarity of stress-strain plots of the pure matrix and the composite shown in *Figures 6-8*. It seems clearly that similar underlying deformation mechanisms in the matrix govern the constitutive behaviour of the test composites.

Therefore, let us use *Equations 1* and *2* to 'fit' the experimentally determined nonlinear rate-dependent compressive yield stress of Plytron. The resulting Eyring plot, for the 45^o off-axis direction, is shown in *Figures 12*. The activation volumes were determined from slopes of least square fits of the linear segments i.e. at quasi-static and high rate arms of the Eyring plots. The two linear asymptotes intersect at a critical stress: $\sigma_Y^{crit} = 105$ MPa and critical strain rate, $\dot{\epsilon}^{crit} = 221s^{-1}$, with the later defining the critical strain rate at which the second process begins to dominate the rate-dependent yielding of the composite. Also, a comparison of the Ree-Eyring profiles of all test directions and the matrix with the yield model prediction based on the *two-process model*, is shown in *Figure 13*.

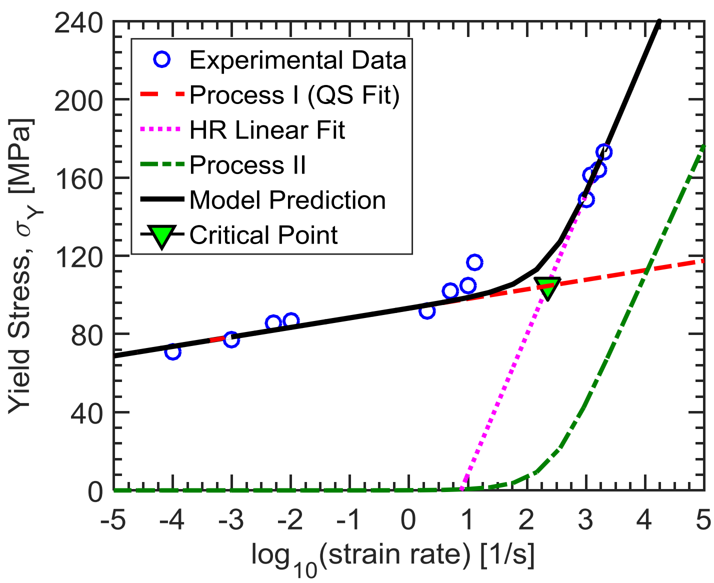

Figure 12: Rate-dependent off-axis response of the test composite: illustrated using *Ree-Eyring* plots for the 45^o test direction.Critical point is: [$\dot{\epsilon}^{crit} = 221s^{-1}$, $\sigma_y^{crit} = 105$ MPa]

By considering the slopes of least-squares fit of linear segments of the Eyring plot (i.e. quasi-static and high rates arm), the dominant activation volumes (V_s and V_p) of each of the processes that act co-operatively to initiate yielding, can be determined [33, 36, 37].

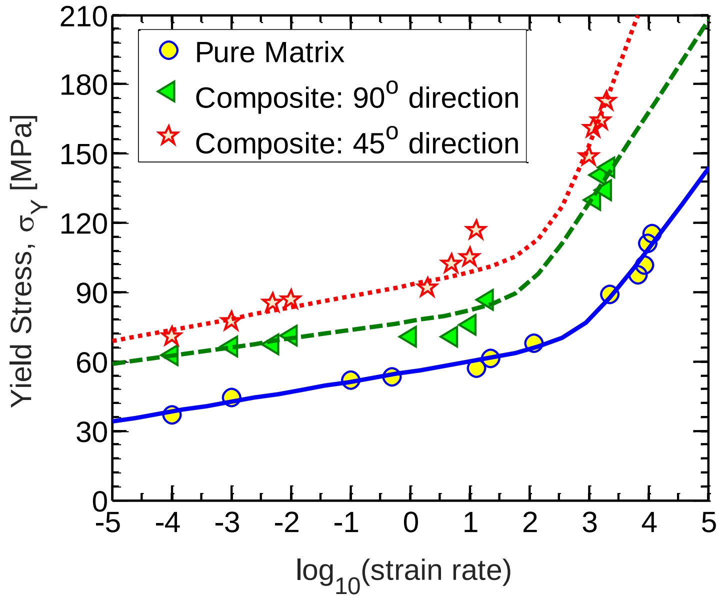

Figure 13: Comparison of Ree-Eyring profiles of the test composite (tested in two off-axis directions) and the pure matrix. *Note: Trend lines on the plot represent model predictions based on the Two-process model formulation* [36].

Table 2 shows that comparison of shear activation volumes for the two test directions of the composite and uniaxial compression of the matrix. Here, the ratio of pressure to shear activation volumes from studies of yield under high pressure is $V_p/V_s \approx 0.07$ [38, 39]. This implies that the ratio of compressive to tensile yield stress for polypropylene is 1.22 according to *Equation 4*.

$$\frac{\sigma_{y,c}}{\sigma_{y,t}} = \frac{1+\sqrt{2}(V_{p,j}/V_{s,j})}{1-\sqrt{2}(V_{p,j}/V_{s,j})} \tag{4}$$

Table 2: A comparison of activation volumes of the composite and pure matrix at quasi-static (process I) and high-rate (process II) regimes.

Test Material	$V_{s,I}$ $[(m^3 mol^{-1})]$	$V_{s,II}$ $[(m^3 mol^{-1})]$	$\dot{\epsilon}^{crit}$ $[s^{-1}]$	σ_y^{crit} [MPa]
Composite: 45^o-direction	2.92×10^{-3}	3.96×10^{-4}	221	105
Composite: 90^o-direction	2.97×10^{-3}	4.07×10^{-4}	80	84
Pure matrix	2.94×10^{-3}	4.62×10^{-4}	655	68

The results from the table show that the rate-dependent off-axis compressive response of Plytron™ follows similar nonlinear function as the bulk matrix, with comparable activation volumes at low and high rates for the two test materials. In effect, the result suggests that the same molecular flow mechanisms govern the rate-dependent compressive yield response of both the matrix and the composite laminate.

5.2. *Rate-dependent Strain Softening*

The effect of test rates on strain softening was also investigated. Strain softening, $\Delta\sigma$ here is defined as the difference between the yield stress, σ_y and the fracture stress, σ_f given by: $\Delta\sigma = |\sigma_y - \sigma_f|$. Results of the pure matrix and the two off-axis test directions of the composite are given in *Figure 14*. At high rates, the material tended to fail prematurely hence we notice a lot of scatter with increasing strain rates for all test materials.

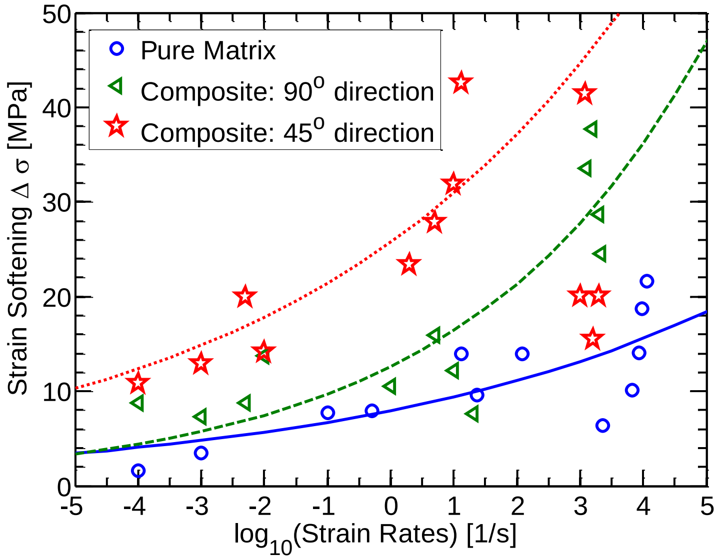

Figure 14: Comparison of rate-dependent strain softening for the pure matrix and the test composite. *Note the trend lines indicate exponential fit of the data.*

A phenomenological model was developed to capture the dependence of strain rate on strain softening as shown by the trend lines in *Figure 14*. The model is defined in *Equation 5*:

$$\Delta\sigma = \Delta\sigma_0 exp(b log_{10}\dot{\epsilon}) \tag{5}$$

where $\Delta\sigma_0$ is a *reference strain softening* at $\dot{\epsilon} = 1\ \mathrm{s}^{-1}$ and b is *time material constant*. *Table 3* shows the values of the different material constants used in generating the trend lines shown in *Figure 14*. The observed strain softening for the test materials was found to increase with strain rate according to a power-law dependence (see *Equation 5*). We note here again that the composite is showing the similar pattern of behaviour to the pure matrix.

Table 3: Table for material constants for the phenomenological strain softening model.

Test Material	σ_0 [MPa]	b [s]
Composite: 45^o-direction	24.19	0.18
Composite: 90^o-direction	15.33	0.24
Pure Matrix	7.95	0.17

5.3. *Rate-dependent fracture response*

The effect of strain rates on fracture strain was also investigated and the results for the pure matrix and the two test directions of the composite are given in *Figure 15*. Results indicate a relationship between fracture strain with strain rate. In fact, as the strain rate increases, the fracture strain for all tested materials decreases steadily as shown in *Figure 15*. The pure matrix data has a lot of scatter since the fracture of the matrix was not consistent as they were very sensitive to test conditions.

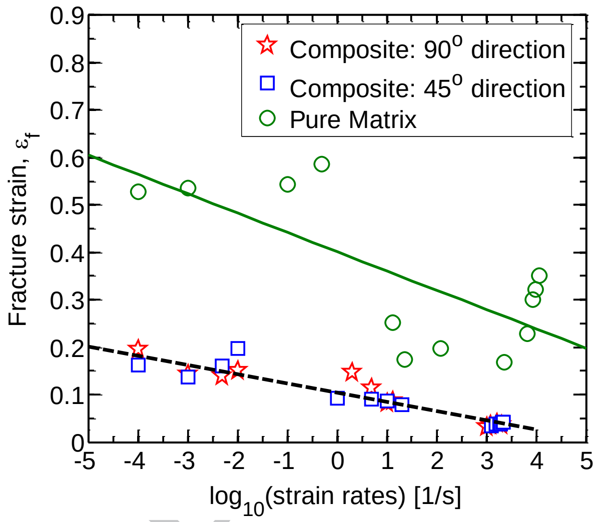

Figure 15: Comparison of rate-dependent fracture strain for the pure matrix and the test composite. *Note the trend lines indicate linear fit of the data.*

6. Visualization of Rate-dependent Compression of the test composite

6.1. *Quasi-static strain rate test images*

Figures 16(a) and *16(b)* show the sequence of images obtained for a quasi-static off-axis compression test in 90^o direction. The dominant failure mechanism is interlaminar matrix failure exhibiting two distinct evolution patterns. *Type I* evolution pattern initiates from the centre of the specimen and evolves leading to an *inverted V-shaped* wedge while *Type II* pattern initiates from the corners of the specimen and the crack travels diagonally through the specimen leading again to an *inverted V-shaped* wedge as shown in *Figure 16*. The evolution of damage for these quasi-static tests is consistently along a clearly defined fracture plane: a feature that is a well known off-axis compressive response of unidirectional composites.

For the off-axis compression in the 45^o-direction, the failure mechanism again is interlaminar matrix failure. However, damage propagation was along the 45^o-fibres as shown in *Figure 17*. We identify two propagation patterns as well, as shown in *Figures 17(a) and 17(b)*.

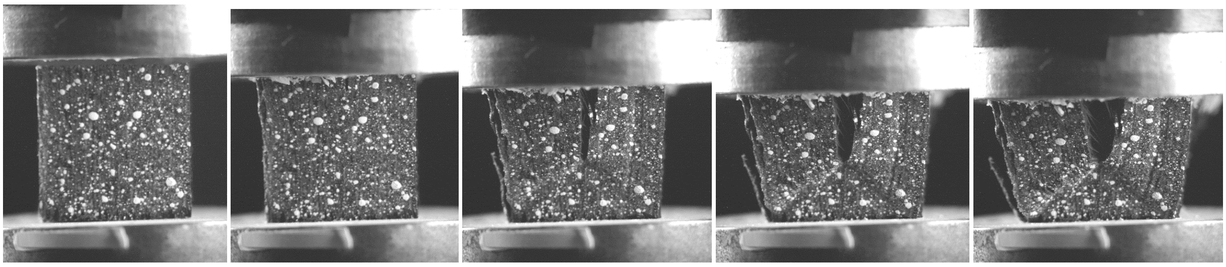

(a) Type I failure mode

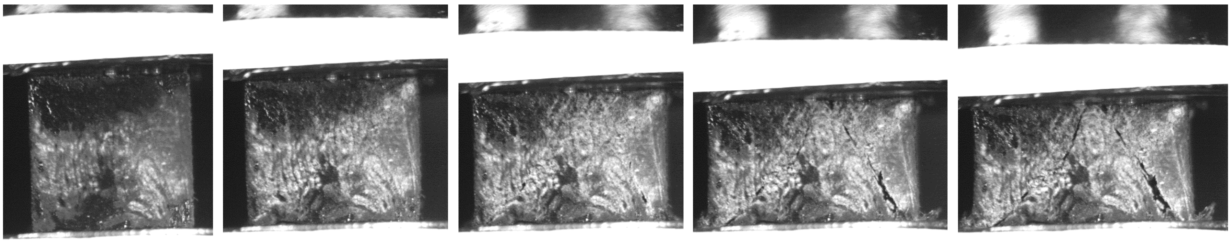

(b) Type II failure mode

Figure 16: Sequence of images showing failure mechanisms obtained from 90^o off-axis compression of Plytron™ tested at *quasi-static rates*. Specimen dimensions are: $10 \times 10 \times 10$ mm^3. Note that the fibres are pointing out of the page.

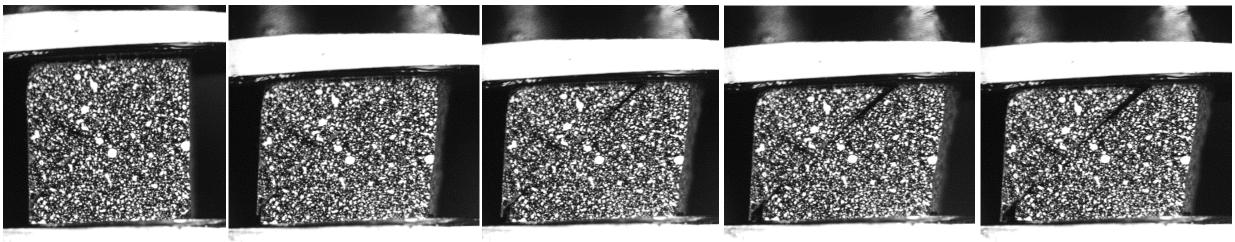

(a) Type III failure mode

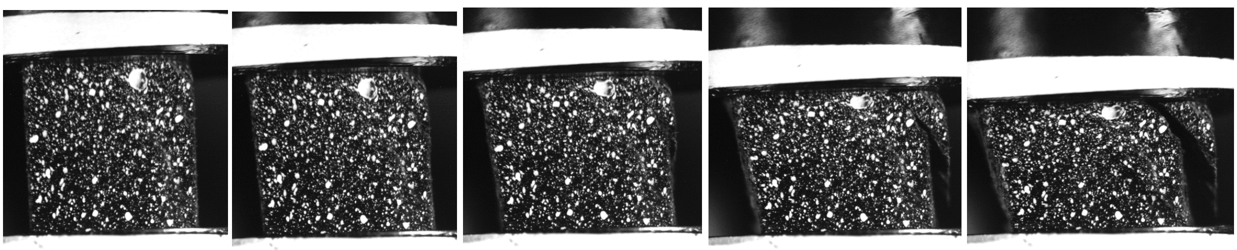

(b) Type IV failure mode

Figure 17: Sequence of images showing failure mechanisms obtained from 45^o-direction off-axis compression of Plytron™ tested at *quasi-static rates*. Specimen dimensions are: $10 \times 10 \times 10$ mm^3. Note that the fibres make angle $\sim 45^o$ with the compression test direction.

6.2. *Medium strain rate test images*

Images from medium rate compressive testing of Plytron are shown in *Figure 18 and 19* for the 90^o- and 45^o-test directions. The images showed that similar interlaminar matrix failure as the quasi-static rates was observed for medium rate test. For the 90^o-direction compression tests, the damage initiation and evolution was consistent with the quasi-static specimen. Unfortunately, at failure, fragments of the failed composites were out of focus as shown in both specimens of *Figure 18*. On the other hand, the 45^o-direction compression tests showed a well-define shear-zone is formed 45^o to the test direction (as shown in *Figure 19*).

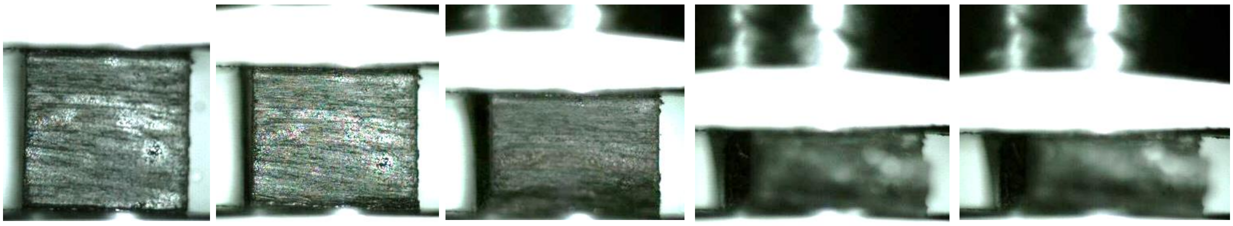

(a) specimen I

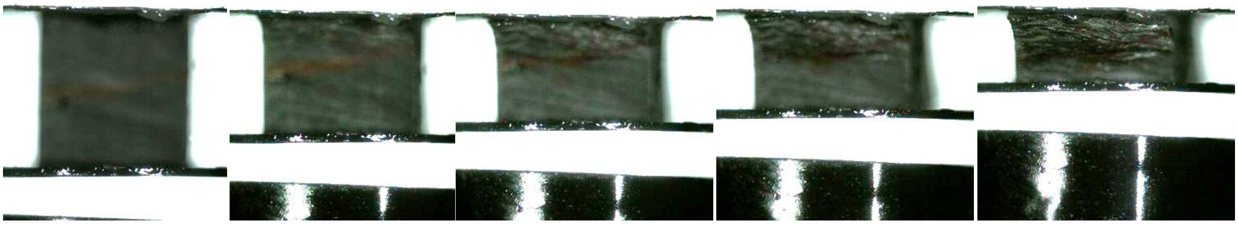

(b) specimen II

Figure 18: Sequence of images showing failure mechanisms obtained from 90^o-direction off-axis compression of Plytron$^{\text{TM}}$ tested at *medium rates*. Specimen dimensions are: $10 \times 10 \times 10$ mm^3. Note that at failure, failed specimens were out of focus hence the blurred images.

6.3. *High strain rate test Images*

Using a Cordion 550 ultrahigh speed camera attached to a compression split Hopkinson pressure bar (SHPB), in situ images were acquired showing the high rate off-axis compressive behaviour of the test composite . The sequence of images from the test are shown in *Figure 20* and *21* for the two off-axis test directions. Although different specimens (of different heights) were also tested particularly for the 45^o-test direction, similar damage evolution patterns were observed. Similar compressive behaviour reported for quasi-static and medium-rate tests was observed for high rate tests. For example, *Figures 20(a)* shows damage evolution along a fracture plane oriented at 45^o, similar to the quasi-static and medium rate compressive behaviour reported earlier. In *Figures 22a-c*, a fracture plane oriented at 45^o to compression direction was observed, similar to the quasi-static and medium strain rates.

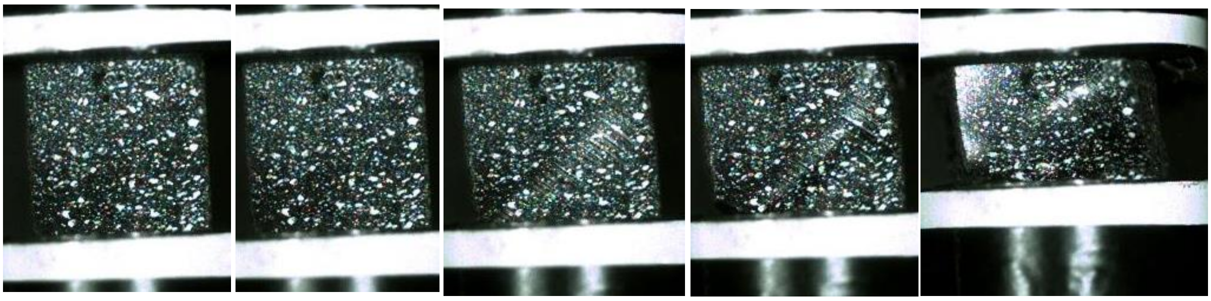

(a)

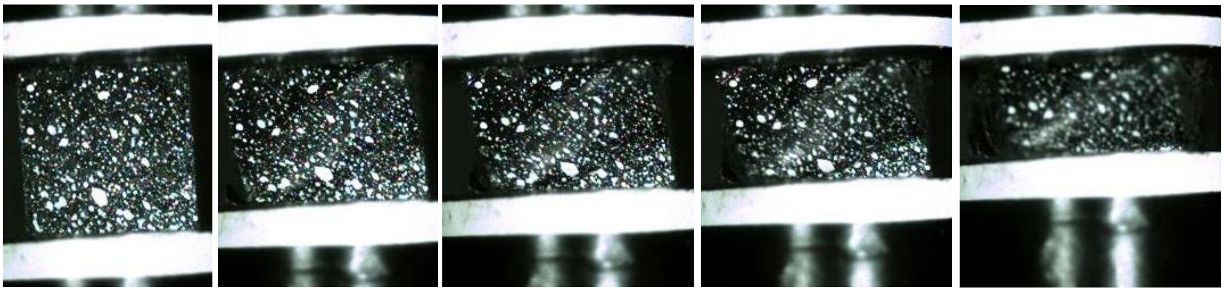

(b)

Figure 19: Sequence of images showing failure mechanisms obtained from 45^o-direction off-axis compression of Plytron™ tested at *medium rates*. Specimen dimensions are: $10 \times 10 \times 10$ mm^3.

However, following initiation of failure at high rates, there is a distinct difference between damage evolution at high rates response and quasi-static or medium rates. The sequence at which the failure modes appeared was observed to be different. As shown in *Figures 23a*, three fracture planes were observed from in situ images of a high rate compression test for nominal strain rate, $\dot{\epsilon} = 2000s^{-1}$. The crack front 1, appeared first and with increasing compression, crack fronts 2 and 3 appeared later. Such a response can be investigated by comparing the images acquired at high rates from $\dot{\epsilon} = 1400s^{-1}$ to $\dot{\epsilon} = 2000s^{-1}$; and secondly investigating the probability of the response being a consequence of the geometry of test specimen. *Figures 23b* and *c* show similar multi-crack-fronts response for a cuboid test specimen of height, $h = 15mm$. In the first instance, the compressive fracture behaviour at strain rate, $\dot{\epsilon} = 1400s^{-1}$, shown in *Figure 22* compared well with those of *Figure 23*. Immediately, the different response with changing strain rates, can be observed. As a result, it is concluded that the presence of many crack fronts or fracture planes at highest rates is a rate-dependent response.

Figure 24 illustrates a peculiarity of the 90^o-direction compressive response where simultaneously activated interlaminar failure modes exist. This is different from the individually singly-activated failure mode seen at quasi-static rates. Further studies are required to explore this effect.

This study has established that at high strain rates, the strength of the matrix is significantly higher than at low rates. Again, the fracture strain of the composite decreases linearly with increasing strain rates. By considering this increased brittleness of the composite and the rate-induced increases in yield stress, a possible explanation for the rate-dependent

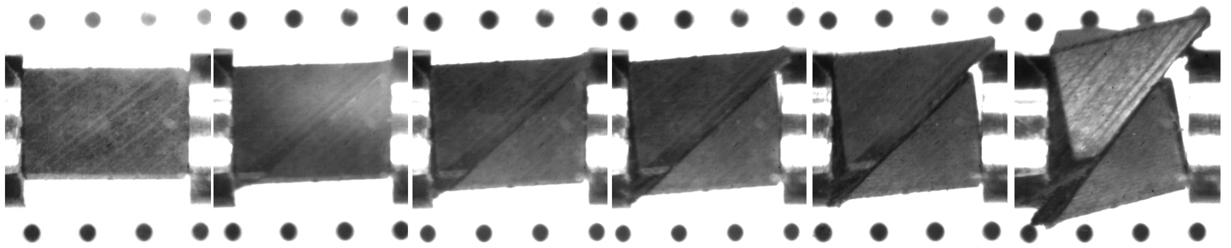

(a) $15 \times 15 \times 10$ mm^3 cubic specimens (plain)

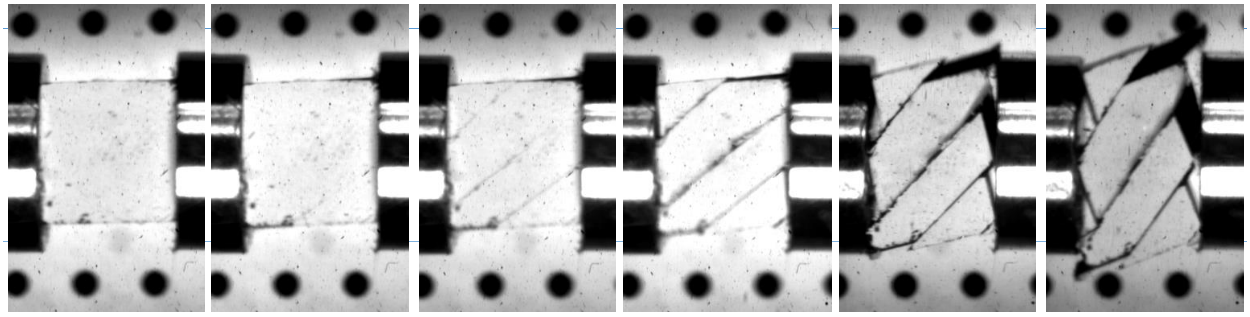

(b) $8 \times 8 \times 8$ mm^3 cubic specimen, with white painting (to highlight cracks)

Figure 20: Sequence of images showing failure mechanisms obtained from 45^o-direction off-axis compression of Plytron$^{\text{TM}}$ tested at *high strain rates*.

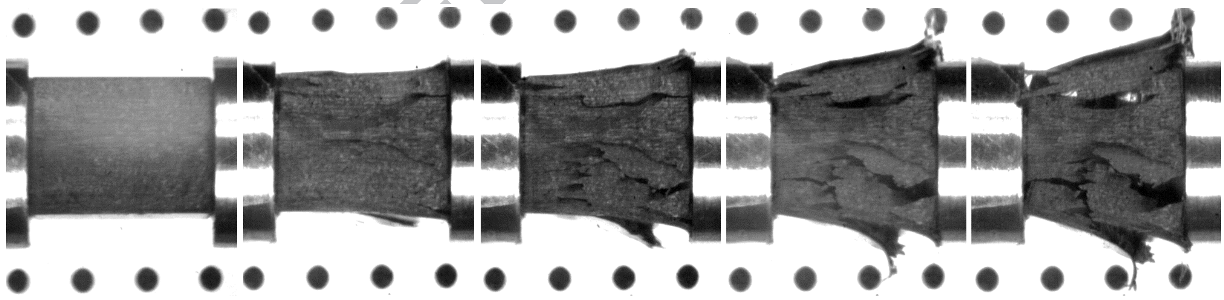

Figure 21: Sequence of images and their failure mechanisms for off-axis compressive response of Plytron$^{\text{TM}}$ tested in 90^o-direction at *high strain rates*.

formation of fracture planes is that there must exist several regions of higher stresses in the composite. These areas can become what is described here as *temporary crack-front arresters* during the propagation of failure. With such temporary suspension of travel of original crack front, new crack fronts develop at regions in the matrix with lower localized stress state than the 'arrested region', thus leading to formation of multiple crack fronts as illustrated in *Figure 23*. With more loading, the new and original crack fronts continue to propagate until total failure of the material.

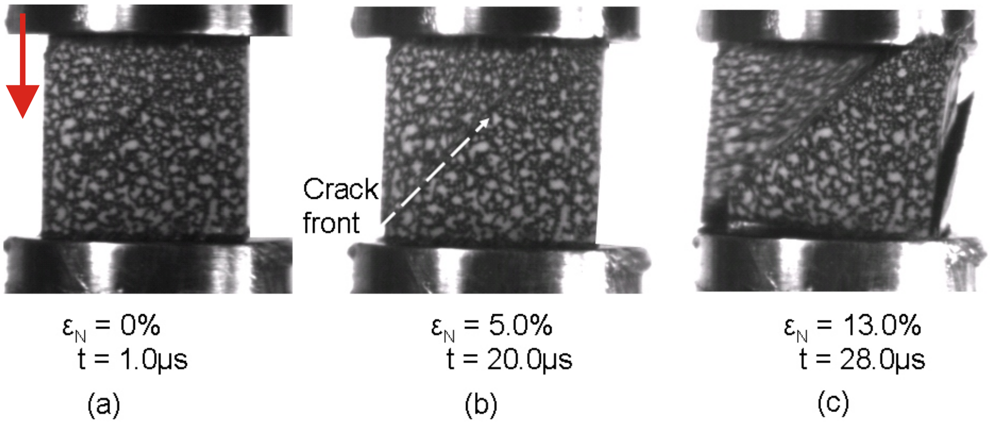

Figure 22: Images sequence for HR off-axis compressive of Plytron™ $[0_{43}]$ laminates at 45^o direction, for strain rate, $\dot{\epsilon} = 1400\ \mathrm{s}^{-1}$.

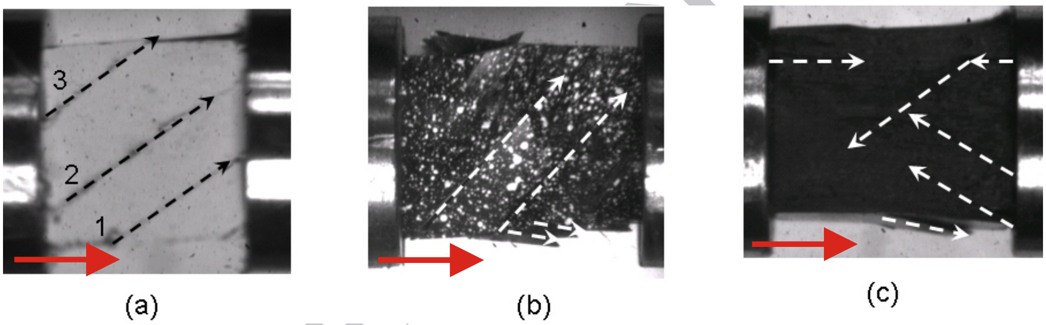

Figure 23: Sequence of failure modes from HR off-axis compression test (on 45^o-specimens) of Plytron™ showing (a) formation of several fracture planes at highest rates with crack fronts 1 appearing first and 3 last, (b & c) formation of several fracture planes for cuboid test specimens of dimensions: length,$d = 10mm$; width, $w = 10mm$ and height, $h = 15mm$. Horizontal red arrow indicates loading direction.

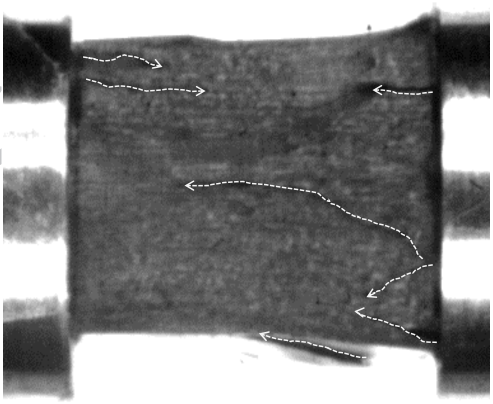

(a) white arrows show crack propagation

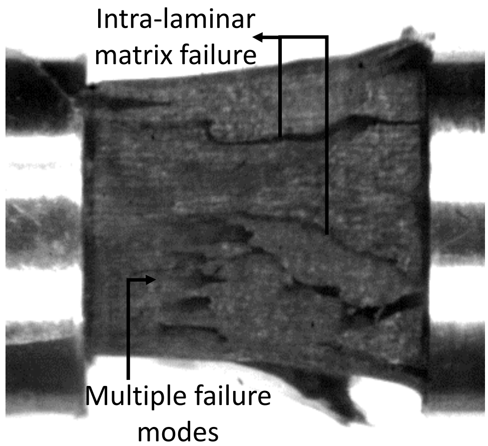

(b) note absence of kink bands

Figure 24: Simultaneously activated multiple failure modes observed in *high strain rate* off-axis compression test along 90^o to the fibre axis.

7. Conclusions

This study has investigated the rate-dependent off-axis compression of an E-glass fibre polypropylene matrix unidirectional composite marketed as Plytron™ . The investigation considered strain rates from quasi-static to high strain rates (i.e. $10^{-3}s^{-1}$ to $10^{3}s^{-1}$). The effect of strain rate on the consitutive behaviour of the test composite was investigated by considering independently the yield, strain softening and fracture strain of the composite. The results of the test composite were compared with the rate-dependent response of the pure matrix used in the test composite and it was concluded that the effect of the matrix was central to the observed rate-dependent behaviour of the test composite. A *Ree-Eyring* style yield model for the test composite was developed based on the underlying molecular kinetics of the pure matrix. Both model predictions and experiments were found to agree very well. A phenomenological strain softening model for the test composite was also developed. The study concludes that the strain softening observed in off-axis compression of the composite increases as a power law in strain rates. Finally, the study concluded that the fracture strain decreases linearly with increasing strain rates.

With aid of a image acquisition kit attached to the test apparatus at both quasi-static, medium and high strain rate, *in situ* images of the deforming composite were derived. These gave evidence of the underlying failure mechanisms. For example, the evolution of damage for quasi-static and medium strain rate tests was consistently along a clearly defined fracture plane. However,the study showed a rate-dependent evolution of damage manifested by the presence of many crack fronts or fracture planes at highest rates. The authors suggest that the rate-induced increases in yield stress and the increasing brittleness of the composite contribute to create the multiple crack fronts seen at high rates.

The results presented in this study and the different models proposed to capture different aspects of the constitutive behaviour of the composite provide evidence for further micromechanical model development of a macroscale constitutive model for the test composite. Results will also provide model development data for finite element studies of finitely deforming polymer reinforced composites. Further compression tests along fibre direction and on angle-ply composites will provide complementary evidence of the underlying mechanisms of compression of such composites.

References

References

[1] Campbell, K.W., Mott, P.H.. Damage tolerance in glass reinforced polymer laminates. Composites Science and Technology 2014;95:21–28. doi:\bibinfo{doi}{10.1016/j.compscitech.2014.02.004}. URL http://www.sciencedirect.com/science/article/pii/S0266353814000505.

[2] Naik, N., Venkateswara Rao, K., Veerraju, C., Ravikumar, G.. Stressstrain behavior of composites under high strain rate compression along thickness direction: Effect of loading condition. Materials & Design 2010;31(1):396–401. doi:\bibinfo{doi}{10.1016/j.matdes.2009.06.005}. URL http://www.sciencedirect.com/science/article/pii/S0261306909002817.

[3] Cogswell, F.. The experience of thermoplastic structural composites during processing. Composites Manufacturing 1991;2(3-4):208–216. doi:\bibinfo{doi}{10.1016/0956-7143(91)90142-4}. URL http://www.sciencedirect.com/science/article/pii/0956714391901424.

[4] Gibson, A., Må nson, J.A.. Impregnation technology for thermoplastic matrix composites. Composites Manufacturing 1992;3(4):223–233. doi:\bibinfo{doi}{10.1016/0956-7143(92)90110-G}. URL http://www.sciencedirect.com/science/article/pii/095671439290110G.

[5] Miller, A., Dodds, N., Hale, J., Gibson, A.. High speed pultrusion of thermoplastic matrix composites. Composites Part A: Applied Science and Manufacturing 1998;29(7):773–782. doi:\bibinfo{doi}{10.1016/S1359-835X(98)00006-2}. URL http://www.sciencedirect.com/science/article/pii/S1359835X98000062.

[6] Ageorges, C., Ye, L., Hou, M.. Advances in fusion bonding techniques for joining thermoplastic matrix composites: a review. Composites Part A: Applied Science and Manufacturing 2001;32(6):839–857. doi:\bibinfo{doi}{10.1016/S1359-835X(00)00166-4}. URL http://www.sciencedirect.com/science/article/pii/S1359835X00001664.

[7] Harte, A., Mc Namara, J.. Overinjection of thermoplastic composites. Journal of Materials Processing Technology 2007;182(1-3):12–20. doi:\bibinfo{doi}{10.1016/j.jmatprotec.2006.06.016}. URL http://www.sciencedirect.com/science/article/pii/S0924013606006510.

[8] van Rijswijk, K., Bersee, H.. Reactive processing of textile fiber-reinforced thermoplastic composites An overview. Composites Part A: Applied Science and Manufacturing 2007;38(3):666–681. doi:\bibinfo{doi}{10.1016/j.compositesa.2006.05.007}. URL http://www.sciencedirect.com/science/article/pii/S1359835X06002247.

[9] Govender, R.A., , Langdon, G.S., , Cloete, T.J., , Nurick, G.N., . High strain rate compression testing of glass fibre reinforced polypropylene. EPJ Web of Conferences 2012;26:01039. doi:\bibinfo{doi}{10.1051/epjconf/20122601039}. URL http://dx.doi.org/10.1051/epjconf/20122601039.

[10] Fitoussi, J., Bocquet, M., Meraghni, F.. Effect of the matrix behavior on the damage of ethylene-propylene glass fiber reinforced composite subjected to high strain rate tension. Composites Part B: Engineering 2013;45(1):1181–1191. doi:\bibinfo{doi}{10.1016/j.compositesb.2012.06.011}. URL http://www.sciencedirect.com/science/article/pii/S1359836812004209.

[11] Carrillo, J.G., Gamboa, R.A., Flores-Johnson, E.A., Gonzalez-Chi, P.I.. Ballistic performance of thermoplastic composite laminates made from aramid woven fabric and polypropylene matrix. Polymer Testing 2012;31(4):512–519.

[12] González, C., Llorca, J.. Mechanical behavior of unidirectional fiber-reinforced polymers under transverse compression: Microscopic mechanisms and modeling. Composites Science and Technology 2007;67(13):2795–2806. URL http://www.sciencedirect.com/science/article/B6TWT-4N2D2XH-6/2/086e971fb4b6fed8706f187b0c147732.

[13] Koerber, H., Camanho, P.. High strain rate characterisation of unidirectional carbonepoxy IM7-8552 in longitudinal compression. Composites Part A: Applied Science and Manufacturing 2011;42(5):462–470. doi:\bibinfo{doi}{10.1016/j.compositesa.2011.01.002}. URL http://www.sciencedirect.com/science/article/pii/S1359835X11000054.

[14] Melro, A., Camanho, P., Andrade Pires, F., Pinho, S.. Micromechanical analysis of polymer composites reinforced by unidirectional fibres: Part II Micromechanical analyses. International Journal of Solids and Structures 2013;50(11-12):1906–1915. doi:\bibinfo{doi}{10.1016/j.ijsolstr.2013.02.007}. URL http://www.sciencedirect.com/science/article/pii/S0020768313000723.

[15] Melro, A., Camanho, P., Andrade Pires, F., Pinho, S.. Micromechanical analysis of polymer composites reinforced by unidirectional fibres: Part I Constitutive modelling. International Journal of Solids and Structures 2013;50(11-12):1897–1905. doi:\bibinfo{doi}{10.1016/j.ijsolstr.2013.02.009}. URL http://www.sciencedirect.com/science/article/pii/S0020768313000747.
[16] Tan, W., Falzon, B.G., Chiu, L.N., Price, M.. Predicting low velocity impact damage and Compression-After-Impact (CAI) behaviour of composite laminates. Composites Part A: Applied Science and Manufacturing 2015;71:212–226. doi:\bibinfo{doi}{10.1016/j.compositesa.2015.01.025}. URL http://www.sciencedirect.com/science/article/pii/S1359835X15000366.
[17] Brown, K.A., Brooks, R., Warrior, N.A.. The static and high strain rate behaviour of a commingled E-glass/polypropylene woven fabric composite. Composites Science and Technology 2010;70(2):272–283. doi:\bibinfo{doi}{10.1016/j.compscitech.2009.10.018}. URL http://www.sciencedirect.com/science/article/pii/S0266353809003819.
[18] Hufenbach, W., Böhm, R., Thieme, M., Winkler, A., Mäder, E., Rausch, J., et al. Polypropylene/glass fibre 3D-textile reinforced composites for automotive applications. Materials & Design 2011;32(3):1468–1476. doi:\bibinfo{doi}{10.1016/j.matdes.2010.08.049}. URL http://www.sciencedirect.com/science/article/pii/S0261306910005388.
[19] GuritSuprem, . Material safety data sheet - plytron: According to ec directive 91/155/eec. Tech. Rep.; GuritSuprem; 2004.
[20] GuritSuprem, . Plytron - product description, properties and applications - a technical report. Tech. Rep.; Gurit Composite Technologies; 2005.
[21] Cogswell, F.N., Meakin, P.J., Staniland, P.A.. Fibre reinforced stuctural thermoplastic composite materials. 1993. US Patent 5,219,642.
[22] Zhao, H., Gary, G.. A new method for the separation of waves. Application to the SHPB technique for an unlimited duration of measurement. Journal of the Mechanics and Physics of Solids 1997;45(7):1185–1202. URL http://www.sciencedirect.com/science/article/B6TXB-3SPKT67-7/2/9ee81c6c784501e4b5c90ef21d835b58.
[23] Bacon, C.. Separation of waves propagating in an elastic or viscoelastic Hopkinson pressure bar with three-dimensional effects. International Journal of Impact Engineering 1999;22(1):55–69. doi:\bibinfo{doi}{10.1016/S0734-743X(98)00048-7}. URL http://www.sciencedirect.com/science/article/pii/S0734743X98000487.
[24] Bussac, M.N., Collet, P., Gary, G., Othman, R.. An optimisation method for separating and rebuilding one-dimensional dispersive waves from multi-point measurements. Application to elastic or viscoelastic bars. Journal of the Mechanics and Physics of Solids 2002;50(2):321–349. doi:\bibinfo{doi}{10.1016/S0022-5096(01)00057-6}. URL http://www.sciencedirect.com/science/article/pii/S0022509601000576.
[25] Siviour, C.R., Jordan, J.L.. High strain rate mechanics of polymers: A review. Journal of Dynamic Behavior of Materials 2016;2(1):15–32. doi:\bibinfo{doi}{10.1007/s40870-016-0052-8}. URL http://dx.doi.org/10.1007/s40870-016-0052-8.
[26] Park, S., Zhou, M.. Separation of elastic waves in split hopkinson bars using one-point strain measurements. Experimental Mechanics 1999;39(4):287–294. doi:\bibinfo{doi}{10.1007/BF02329807}. URL http://dx.doi.org/10.1007/BF02329807.
[27] Okereke, M.I., Buckley, C.P., Siviour, C.R.. Compression of polypropylene across a wide range of strain rates. Mechanics of Time-Dependent Materials, DOI: 101007/s11043-012-9167-z 2012;:1–19doi:\bibinfo{doi}{10.1007/s11043-012-9167-z}. URL http://dx.doi.org/10.1007/s11043-012-9167-z.
[28] Taniguchi, N., Nishiwaki, T., Hirayama, N., Nishida, H., KawadaA, H.. Dynamic tensile properties of carbon fiber composite based on thermoplastic epoxy resin loaded in matrix-dominant directions. Composites Science and Technology 2009;69(2):207–213. doi:\bibinfo{doi}{10.1016/j.compscitech.2008.10.002}. URL http://www.sciencedirect.com/science/article/pii/S0266353808004077.
[29] Gómez-del Río, T., Rodríguez, J., Pearson, R.. Compressive properties of nanoparticle modified epoxy resin at different strain rates. Composites Part B: Engineering 2014;57:173–179. doi:\bibinfo{doi}{10.1016/j.compositesb.2013.10.002}. URL http://www.sciencedirect.com/science/article/pii/S1359836813005672.
[30] Ree, T.S., Ree, T., Eyring, H., Fueno, T.. Activated complexes of fast bimolecular reactions. The Journal of Chemical Physics 1962;36(1).

[31] Mulliken, A., Boyce, M.. Mechanics of the rate-dependent elasticplastic deformation of glassy polymers from low to high strain rates. International Journal of Solids and Structures 2006;43(5):1331 – 1356. doi:\bibinfo{doi}{http://dx.doi.org/10.1016/j.ijsolstr.2005.04.016}. URL http://www.sciencedirect.com/science/article/pii/S0020768305002313.

[32] Richeton, J., Ahzi, S., Vecchio, K., Jiang, F., Adharapurapu, R.. Influence of temperature and strain rate on the mechanical behavior of three amorphous polymers: Characterization and modeling of the compressive yield stress. International Journal of Solids and Structures 2006;43(78):2318 – 2335. doi:\bibinfo{doi}{http://dx.doi.org/10.1016/j.ijsolstr.2005.06.040}. URL http://www.sciencedirect.com/science/article/pii/S0020768305003677.

[33] Buckley, C.P., Dooling, P.J., Harding, J., Ruiz, C.. Deformation of thermosetting resins at impact rates of strain. Part 2: constitutive model with rejuvenation. Journal of the Mechanics and Physics of Solids 2004;52(10):2355–2377. URL http://www.sciencedirect.com/science/article/pii/S0022509604000742.

[34] Siviour, C., Walley, S., Proud, W., Field, J.. The high strain rate compressive behaviour of polycarbonate and polyvinylidene difluoride. Polymer 2005;46(26):12546 – 12555. doi:\bibinfo{doi}{http://dx.doi.org/10.1016/j.polymer.2005.10.109}. URL http://www.sciencedirect.com/science/article/pii/S0032386105015806.

[35] Hull, D., Clyne, T.W.. An Introduction to Composite Materials. Cambridge Solid State Science Series; Cambridge: Cambridge University Press; 1996. ISBN 9780521388559. URL https://books.google.co.uk/books?id=BRcdDu4bUhMC.

[36] Okereke, M.I., Le, C.H., Buckley, C.P.. A new constitutive model for prediction of impact rates response of polypropylene. In: DYMAT2012 - 10th International DYMAT Conference. EPJ Web of Conferences; 2012,.

[37] Wu, J.J., Buckley, C.P.. Plastic deformation of glassy polystyrene: A unified model of yield and the role of chain length. Journal of Polymer Science Part B: Polymer Physics 2004;42(11):2027–2040. doi:\bibinfo{doi}{10.1002/polb.20089}. URL http://dx.doi.org/10.1002/polb.20089.

[38] Joseph, S.H., Duckett, R.A.. Effects of pressure on the non-linear viscoelastic behaviour of polymers: 1. Polypropylene. Polymer 1978;19(7):837–843. URL http://www.sciencedirect.com/science/article/B6TXW-48FC01M-1MJ/2/ef75671bb94f233c2a3a916714499d17.

[39] Yoon, H.N., Pae, K.D., Sauer, J.A.. The effects of combined pressuretemperature on mechanical behavior of polypropylene. Journal of Polymer Science: Polymer Physics Edition 1976;14(9):1611–1627. doi:\bibinfo{doi}{10.1002/pol.1976.180140908}. URL http://dx.doi.org/10.1002/pol.1976.180140908.